

Covert Communications for Intelligent Reflecting Surface-Enabled D2D Networks

Yihuai Yang, Bin Yang, Shikai Shen, Yumei She, Xiaohong Jiang and Tarik Taleb

Abstract—In this paper, we explore covert communications in a device-to-device (D2D) network consisting of an intelligent reflecting surface (IRS), a base station, a cellular user, a D2D pair, and an adversary warden. With the help of the IRS, the D2D pair attempts to perform covert communication, while the warden also tries to detect the very existence of such a transmission. To investigate the covert performance under the scenario, we derive the detection error probability at Warden, the optimal detection threshold for minimizing the probability, and the transmission outage probabilities for D2D and cellular communications, respectively. We further jointly optimize the transmission powers of the cellular user and the D2D transmitter, the reflection phase shifts, and the amplitudes of the IRS reflecting elements to improve covert communication performance. Finally, we provide numerical results to reveal the impact of system parameters on the covert performance and also to exhibit the merits of IRS-enabled D2D networks for achieving covert communications.

Keywords—D2D network, IRS, covert communications, performance analysis.

This work is supported in part by the National Natural Science Foundation of China (62372076); in part by the Academician Weiming Shen Workstation, Yunnan, China (202505AF350084); in part by the Joint Fund for Basic Research of Local Universities in Yunnan Province (202401BA070001-109, 202101BA070001-150, 202101BA070001-088); in part by the Yunnan Key Laboratory of Intelligent Logistics Equipment and Systems; in part by the Education Department Research Foundation of Anhui Province (DTR2023051, 2023AH051593, 2022AH051097); in part by the Innovation Research Team on Future Network Technology of Chuzhou University; in part by the Innovation Team on Smart Home Appliance Security and Applications of Chuzhou City; in part by the Innovative Research Team on Application of Big Data and Financial Technology of Chuzhou University; in part by the ICTFICIAL Oy, Finland; in part by the European Union's HE Research and Innovation Program HORIZON-JUSNS-2023 through the 6G-Path (101139172); in part by the Science and Technology Projects of Yunnan Universities Serving Key Industries (FWCY-QYCT2024016); in part by the Frontier Research Team of Kunming University (XJ20230043); in part by the Yunnan Science and Technology Innovation Base Construction Project (202407AB110006); in part by the Yunnan Dagan Laboratory Project (YNDG202401ZN01); and in part by the Yunnan Science and Technology Talent Program (202305AC160049). (Corresponding author: Shikai Shen, Bin Yang).

Yihuai Yang is with the School of Information Engineering, Kunming University, Yunnan 650214, China (e-mail: Yihuai_Yang@126.com).

Bin Yang is with the School of Computer and Information Engineering, Chuzhou University, Chuzhou 239000, China (e-mail: yangbinchi@gmail.com).

Shikai Shen is with the School of Information Engineering, Kunming University, Yunnan 650214, China, and also with the Academician Weiming Shen Workstation, Yunnan 650214, China (e-mail: kmssk2000@sina.com).

Yumei She is with the School of Mathematics and Computer Science, Yunnan Minzu University, and Yunnan Key Laboratory of Smart City and Cyberspace Security, Yunnan 650500, China (e-mail: sheym1965@126.com).

Xiaohong Jiang is with the School of Systems Information Science, Future University Hakodate, Hokkaido 041-8655, Japan (e-mail: jiang@fun.ac.jp).

Tarik Taleb is with the Electrical Engineering and Information Technology, Ruhr University Bochum (RUB), Bochum 44801, Germany (e-mail: taleb-tarik@gmail.com).

I. INTRODUCTION

In device-to-device (D2D) networks, proximity terminals can utilize the spectrum resources of the cellular system to realize direct communication without traversing the base station (BS). D2D networks exhibit many promising features such as improving spectrum efficiency, increasing transmission rate, extending cellular coverage, and offloading BS traffic [1]–[4], which have been identified as a key technology satisfying the ever-increasing traffic demands for massive mobile terminals in the next generation mobile communication systems [5]. Because of the openness and broadcast nature of the wireless medium, D2D networks are facing great security challenges in the wireless transmission of various confidential and sensitive data (e.g., e-health records, financial details) [6].

In the past two decades, traditional cryptographic techniques have been widely adopted to provide protection against eavesdropping. However, such cryptographic techniques are likely to become ineffective when an adversary has high computation capabilities. In recent years, it has been shown that secure communication techniques leverage the randomness and noise of wireless channels to prevent adversaries from eavesdropping on the content of wireless transmissions. However, these techniques do not guarantee protection against malicious detection of signals. As an alternative, covert communication techniques are emerging as a new security paradigm that aims to conceal the very existence of signal transmissions. This approach holds great potential for applications in military and government contexts [7].

Covert communications have been extensively studied since the pioneering work in [8], with subsequent contributions in [9]–[18]. Previous works often rely on relays and jammers, which can lead to high energy consumption and interference, degrading communication performance. To address these challenges, the intelligent reflecting surface (IRS) has emerged as a promising solution. An IRS is composed of low-cost reflecting elements that adjust their amplitudes and phase shifts to dynamically reconfigure the wireless environment. This capability allows IRS technology to enhance legitimate signals and suppress interference [19], [20]. The potential of IRS to improve covert communication performance has been demonstrated in studies such as [21]–[26]. By manipulating signals through IRS, these systems can obscure both the source and nature of communications, significantly enhancing security and privacy. This is especially valuable in military and governmental contexts, where protecting sensitive information and concealing the identities and locations of personnel is critical. While D2D networks have been extensively studied in

TABLE I
COMPARISON BETWEEN THE PROPOSED WORK AND THE BASELINE [32]

Feature	This Work	[32]
Channel Fading Model	IRS-related links follow Rician fading; terrestrial links follow Rayleigh fading (hybrid model)	All channels modeled as Rayleigh fading
IRS-Assisted Paths	Includes additional reflection paths: the cellular user \rightarrow IRS \rightarrow the warden and the cellular user \rightarrow IRS \rightarrow the D2D receiver.	The cellular user is positioned far from the IRS; thus, no reflected signals from the cellular user are considered
System Model	All receiving nodes capture both direct and IRS-reflected signals; general multi-path model	Reflected signals only from the D2D sender; IRS reflection considered only for partial paths
IRS Beamforming Strategy	Jointly optimized using a hybrid analytical and gradient descent algorithm to avoid local optima	No global optimization of IRS phase shifts
Detection Modeling	Non-central chi-square distributions; the exponential integral function $Ei(\cdot)$	Central chi-square assumption; simpler exponential-based expressions
Optimization Algorithms	Introduces three iterative optimization algorithms: IRS phase shift (Algorithm 1), cellular power (Algorithm 2), and overall covert rate (Algorithm 3)	No iterative optimization process proposed
Realistic Fading Models	Hybrid Rayleigh & Rician fading modeling	Degrades under strong LoS conditions due to the exclusive use of Rayleigh fading modeling
Simulation Cases Compared	Six scenarios, including additional Rician K -factor settings, a relay, and the baseline from [33]	Only three basic scenarios

prior works [27]–[31], research has primarily focused on spectrum and power resource allocation, sum rate maximization, and secrecy rate. Covert communications in D2D networks remain largely unexplored. Recently, we conducted a study on covertness and secrecy in an untrusted relay-assisted D2D network [27]. In this scenario, a user seeks to covertly transmit a confidential message to a BS with the help of an untrusted relay, while avoiding detection by a warden and preventing the relay from eavesdropping.

However, covert communication within IRS-assisted D2D-enabled cellular networks remains largely unexplored. Motivated by this gap, our work specifically addresses the unique challenges of covert communication in networks where D2D and cellular systems coexist, with a particular emphasis on leveraging IRS to enhance the covertness of D2D communication. Furthermore, we adopt a more realistic channel model: the IRS-to-node channels are assumed to follow a Rician distribution, which captures line-of-sight (LoS) conditions, while the terrestrial channels adhere to Rayleigh fading. This combination of channel models ensures that our approach more accurately reflects real-world scenarios. Building on the foundation of our previous conference paper [32], this work further explores this critical area. Specifically, our previous conference paper [32] only considered a scenario where the cellular user was positioned far from the IRS, making his signal undetectable by the IRS and therefore unable to generate any reflected signals to other nodes. Additionally, it assumed that all channels followed a Rayleigh distribution. In contrast, this paper presents a more general system model where all receiving nodes can capture both the reflected signals from the IRS and the direct signal from the transmitters. We assume that IRS-to-node and node-to-IRS channels follow a Rician distribution. The communication channels between terrestrial nodes continue to follow a Rayleigh distribution, which better reflects real-world conditions. Under these new assumptions, we have re-derived all the relevant formulations in this paper. Table I presents a comparison between our work and the previous study [32].

The main contributions of this paper are summarized as follows.

- We first derive the detection error probability at Warden,

Kevin, which is the sum of the false alarm probability and missed detection probability. Based on this probability, we further derive the corresponding optimal detection threshold.

- We then derive the transmission outage probability from the D2D source Carol to its destination Ethan and that from the cellular user Alex to the BS, respectively. With these probabilities, we develop a theoretical model of the covert rate for the D2D pair.
- We further model the maximization of covert rate as a constrained optimization problem with the constraints given by the covert requirement, the maximum outage probability, and the transmission powers of Carol and Alex. By solving the optimization problem, the maximum covert rate is obtained for the D2D pair.
- Finally, we provide extensive numerical results to illustrate the impact of system parameters on the covert rate performance and also to demonstrate performance enhancement through deploying IRS in D2D networks.

The remainder of the paper is structured as follows: In Section II, we provide a review of the related work. Section III introduces the system model for IRS-aided D2D networks. The derivation of exact expressions for false alarm and missed detection probabilities at warden, along with the optimization of the detection threshold to minimize detection error probability, is presented in Section IV. Section V focuses on the analysis of transmission outage, while Section VI formulates and solves a constrained optimization problem aimed at maximizing the covert rate, including the relevant algorithms. Numerical results are presented in Section VII, and the paper concludes in Section VIII.

II. RELATED WORKS

A. Covert Communication

Covert communication emerged with the pioneering work in [8], which introduced the square root law for covert communications in additive Gaussian white noise (AWGN) channels. According to this law, the achievable covert rate diminishes to zero as the number of channel uses increases indefinitely, highlighting the fundamental trade-off between

communication efficiency and undetectability. This result has since been extended and verified across various other channel models, including the Binary Symmetric Channel (BSC) [9], which models error-prone communication, the Discrete Memoryless Channel (DMC) [10], which encompasses a broad range of communication systems, and the Multiple-Input Multiple-Output (MIMO) AWGN channel [33], which leverages multiple antennas for spatial diversity. In addition, the Poisson Packet Channel (PPC) [34], a model for bursty packet-based networks, has been analyzed, with the covert rates consistently approaching zero as the number of channel uses increases, further reinforcing the implications of the square root law in diverse settings. Building on this foundational work, researchers have explored various techniques to enhance covert communication. In [11] and [12], jammers have been utilized to generate artificial noise, which introduces additional uncertainty to the warden, enabling the achievement of positive covert rates even as the channel usage increases. This method helps to mask the legitimate communication by creating ambiguity for any eavesdropper. Further advancements are seen in [13], which investigates covert communications within a multi-channel slotted ALOHA system, where covert users attempt to access the channel without being detected by the warden. This model introduces an additional layer of complexity, as users must contend with not only the channel conditions but also the slotted access scheme, which helps to mitigate detection. Additionally, [35] delves into the integration of covert communication within Mobile Edge Computing (MEC), addressing the potential for information leakage when offloading computational tasks. By leveraging edge computing resources, covert communication can be further protected from external observation. Moreover, the application of covert communication has extended into relaying networks, with studies examining both two-hop [14]–[16] and multi-hop [17], [18] scenarios, where the signals are relayed across multiple nodes, further complicating the detection process and enabling improved covert communication performance in large-scale networks.

B. IRS-assisted Covert Communication

A variety of studies have explored IRS-aided covert communication in wireless networks, even without the support of a BS [21]–[26]. The authors in [21] focus on jointly optimizing transmission power and IRS reflection properties to improve covert performance, while [22] achieves the maximum covert rate by optimizing the source transmission power and the IRS phase shift.

The work in [23] examines covert performance improvement through IRS-assisted multi-antenna technologies, and [24] investigates the impact of IRS deployment under both scenarios with and without global channel state information (CSI). Additionally, [25] aims to maximize the covert rate by jointly optimizing transmission probability, power, and the IRS reflection matrix. Meanwhile, [26] explores covert rate maximization in a MIMO system with the aid of IRS. In our previous work [32], we examined a scenario where Alex was situated at a distance from the IRS, causing his signals to be

undetectable and preventing the generation of reflected signals, with all channels modeled using a Rayleigh distribution. This work highlighted the challenges of maintaining covert communication in low-reflection scenarios.

Further advancements are seen in [36], which seeks to maximize effective covert throughput by considering different transmit prior probabilities. The study in [37] examines a UAV-IRS-assisted system where randomized IRS phase shifts and a full-duplex legitimate receiver act as a jammer to deceive the warden, enabling covert communication. Additionally, [38] employs a friendly jammer with random power levels to confuse the warden, while [39] explores IRS-aided covert communication based on LoS channels, eliminating the need for instantaneous CSI of IRS channels.

While IRS-aided covert communication has garnered significant attention, the role of IRS in enhancing D2D networks has also been explored extensively. For instance, the authors in [40] propose using IRS to maximize the system’s sum rate while minimizing interference from D2D pairs. The work in [41] introduces IRS for offloading computation tasks in a D2D cooperative computing network, and [42] extends this by using IRS to offload tasks from active users to idle ones. The study in [43] introduces a two-timescale optimization scheme for improving the performance of IRS-aided D2D networks, while [44] maximizes the achievable rate in an IRS-aided D2D network with hardware impairments and phase noise. In [45], a finite blocklength covert NOMA scheme is proposed that leverages IRS/intelligent omni-surfaces (IOS) switching to enhance covertness, with joint optimization of power allocation and blocklength to maximize ECT. The study in [46] explores IRS deployment to improve covert throughput by increasing the detection error probability, again utilizing a Gauss–Poisson process for spatial modeling. In [47], aerial IRSs are deployed to support covert IoT communication, where deep reinforcement learning is employed to jointly optimize UAV trajectories and IRS phase shifts, aiming to balance the trade-off between information freshness and communication covertness. Further, the maximum transmission rate in distributed IRS-aided D2D networks is explored in [48], and throughput maximization is addressed in [49], with [50] focusing on secrecy rate maximization.

III. SYSTEM MODELS AND PERFORMANCE METRICS

A. Network Model

As illustrated in Fig. 1, this paper considers an uplink cellular network, where there is a cellular user Alex, a D2D pair with a source Carol and a destination Ethan, a warden Kevin, and an IRS. In the network, Carol intends to covertly transmit sensitive messages to Ethan with the help of the IRS, while Kevin attempts to detect whether the transmissions from Carol and the IRS occur or not. The direct link from Carol to Ethan is blocked by obstacles (e.g., buildings), and thus Carol can only receive the sensitive message reflected by the IRS. The IRS includes N passive reflecting elements, each of which can dynamically adjust its phase shift and amplitude to fit the current propagation environment. The BS is equipped with multiple antennas; however, only one of them is involved in our system.

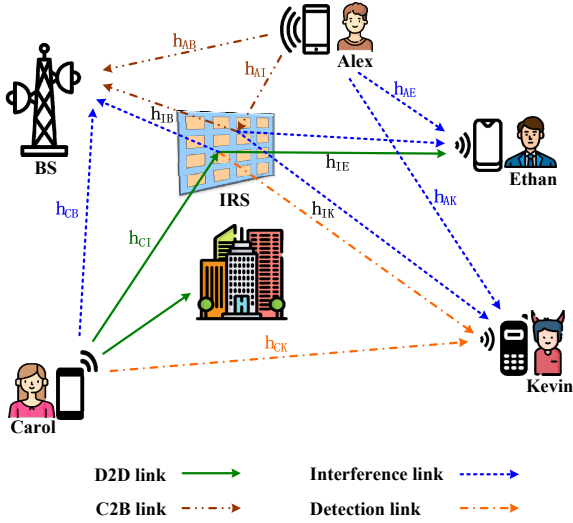


Fig. 1. System Model

B. Channel Model

In our concerned network, there exist ten wireless links, namely, the IRS-to-Ethan link, IRS-to-BS link, IRS-to-Kevin link, Carol-to-IRS link, Carol-to-Kevin link, Carol-to-BS link, Alex-to-BS link, Alex-to-Ethan link, Alex-to-IRS link, and Alex-to-Kevin link, which are represented as \mathbf{h}_{IE} , \mathbf{h}_{IB} , \mathbf{h}_{IK} , \mathbf{h}_{CI} , h_{CK} , h_{CB} , h_{AB} , h_{AE} , \mathbf{h}_{AI} , and h_{AK} , respectively. In this work, the instantaneous CSI of all links, excluding those associated with Kevin, is assumed to be perfectly known at the corresponding nodes via pilot-based estimation and channel reciprocity. For the links involving Kevin (i.e., \mathbf{h}_{IK} , h_{CK} , and h_{AK}), only the statistical CSI is assumed to be available, since Carol, Alex, and the IRS do not transmit pilot signals toward Kevin to avoid exposing covert transmissions.

For the IRS-to-node and node-to-IRS links, such as the IRS-to-Ethan, IRS-to-BS, and Alex-to-IRS links, the channel fading adheres to a Rician distribution. This is because the IRS is typically deployed on the outer wall of a high building, providing a strong LoS link between the IRS and the nodes. The channel characterization for these links is given by:

$$\mathbf{h}_{XY} = \sqrt{\frac{K_{XY}}{1+K_{XY}}} \mathbf{h}_{\text{LoS}} + \sqrt{\frac{1}{1+K_{XY}}} \mathbf{h}_{\text{NLoS}}, \quad (1)$$

where $X, Y \in \{I, A, B, C, E, K\}$. In this expression, K_{XY} represents the Rician factor, \mathbf{h}_{LoS} denotes the LoS component, and \mathbf{h}_{NLoS} represents the non-line-of-sight (NLoS) component.

The LoS component, \mathbf{h}_{LoS} , is determined by the direct, unobstructed path between the transmitter and receiver. It is typically modeled as a deterministic or fixed value, which can be expressed as:

$$\mathbf{h}_{\text{LoS}} = \exp(j\phi_{XY}), \quad (2)$$

where ϕ_{XY} is the phase shift associated with the LoS path, often related to the distance and relative motion between the transmitter and receiver. And, the NLoS component, \mathbf{h}_{NLoS} , typically follows a complex Gaussian distribution, denoted as $\mathcal{CN}(0, \sigma_{XY}^2)$.

On the other hand, the channel fading follows a Rayleigh distribution for the terrestrial node-to-node links, such as Carol-to-Kevin, Carol-to-BS, and Alex-to-BS. Besides, we use σ_X^2 to denote the variance of the additive white Gaussian noise at node X . Under this model, each channel remains unchanged within a single time slot but varies independently across different time slots [51] [52].

C. Transmission from Carol to Ethan

We use P_C and P_A to represent the transmission powers of Carol and Alex, respectively. $x(i)$ and $z(i)$ represent the transmission signals of Carol and Alex, respectively. These signals are independent Gaussian random variables with mean zero and unit variance, i.e., $x(i), z(i) \sim \mathcal{CN}(0, 1)$. Both $E[x(i)x^\dagger(i)]$ and $E[z(i)z^\dagger(i)]$ are equal to 1. Here, $i \in \{1, 2, \dots, L\}$, and the number of wireless channel uses $L \rightarrow \infty$.

When Carol transmits a message at time slot- i , the signal received by Ethan at the i -th channel use is expressed as:

$$y_E(i) = \sqrt{P_C} \mathbf{h}_{IE}^T \Theta \mathbf{h}_{CI} x(i) + \sqrt{P_A} (h_{AE} + \mathbf{h}_{IE}^T \Theta \mathbf{h}_{AI}) z(i) + n_E(i), \quad (3)$$

where, Θ is a diagonal matrix with $N \times N$ dimension, storing the IRS's reflection phase and amplitude information. Θ equals to $\text{diag}(q_1 e^{j\theta_1}, q_2 e^{j\theta_2}, \dots, q_N e^{j\theta_N})$, where the reflection amplitude of the n -th element q_n belongs to $[0, 1]$, and the phase shift belongs to $[0, 2\pi)$.

In equation (3), the first term represents the signal from Carol to Ethan via the IRS. The second term includes both the direct and IRS-reflected signals from Alex to Ethan. The third term is the additive white Gaussian noise (AWGN) at Ethan, where $n_E(i) \sim \mathcal{CN}(0, \sigma_E^2)$.

Then, the SINR, κ_E , at Ethan can be expressed as:

$$\kappa_E = \frac{P_C |\mathbf{h}_{IE}^T \Theta \mathbf{h}_{CI}|^2}{P_A (|h_{AE} + \mathbf{h}_{IE}^T \Theta \mathbf{h}_{AI}|^2) + \sigma_E^2}, \quad (4)$$

where σ_E^2 represents the noise variance at Ethan.

We consider that a received signal at Ethan can be decoded successfully if and only if the rate from Carol to Ethan $\log_2(1 + \kappa_E)$ is no smaller than some threshold value R_{CE} . This means that an outage occurs if the rate is smaller than R_{CE} . In this paper, we use outage probability to represent the probability that the outage occurs.

D. Transmission from Alex to BS

When Alex transmits messages at some time slot- i , the received signal $y_B(i)$ at the BS can be expressed as:

$$y_B(i) = \sqrt{P_A} (h_{AB} + \mathbf{h}_{IB}^T \Theta \mathbf{h}_{AI}) z(i) + \sqrt{P_C} (h_{CB} + \mathbf{h}_{IB}^T \Theta \mathbf{h}_{CI}) x(i) + n_B(i), \quad (5)$$

The term $\sqrt{P_A} (h_{AB} + \mathbf{h}_{IB}^T \Theta \mathbf{h}_{AI}) z(i)$ represents the signal received from Alex, which includes both the direct and IRS-reflected components. This is the desired signal at the BS for cellular communication. Meanwhile, the term $\sqrt{P_C} (h_{CB} + \mathbf{h}_{IB}^T \Theta \mathbf{h}_{CI}) x(i)$ represents the signal received from Carol, also including both the direct and IRS-reflected components; however, it acts as interference for the BS in cellular communication. Additionally, $n_B(i)$ denotes the additive white Gaussian noise (AWGN) at the BS, where $n_B(i) \sim \mathcal{CN}(0, \sigma_B^2)$.

Then, we express the SINR κ_B at BS as

$$\kappa_B = \frac{P_A |h_{AB} + \mathbf{h}_{IB}^T \Theta \mathbf{h}_{AI}|^2}{P_C |h_{CB} + \mathbf{h}_{IB}^T \Theta \mathbf{h}_{CI}|^2 + \sigma_B^2}, \quad (6)$$

where σ_B^2 represents the noise variance at BS.

We consider that an outage will not occur when the rate from Alex to BS $\log_2(1 + \kappa_B)$ is no smaller than some threshold value R_{AB} .

IV. DETECTION PERFORMANCE AT KEVIN

In this section, we analyze the hypothesis test at Kevin and derive the probabilities of false alarm and missed detection. We then determine the optimal detection threshold to minimize the detection error probability.

A. Hypothesis Testing at Kevin

At each time slot, the warden Kevin detects whether or not Carol transmits messages to Ethan. Thus, Kevin needs to do a binary hypothesis testing [52]. We use \mathcal{H}_1 to represent the alternative hypothesis, corresponding to the case that Carol transmits messages. On the other hand, we use \mathcal{H}_0 to represent the null hypothesis, which means that Carol does not transmit messages. Under these two hypotheses, the received signal at Kevin can be expressed as

$$y_K(i) = \begin{cases} \sqrt{P_A} (h_{AK} + \mathbf{h}_{IK}^T \Theta \mathbf{h}_{AI}) z(i) + n_K(i), & \mathcal{H}_0 \\ \sqrt{P_C} (h_{CK} + \mathbf{h}_{IK}^T \Theta \mathbf{h}_{CI}) x(i) \\ + \sqrt{P_A} (h_{AK} + \mathbf{h}_{IK}^T \Theta \mathbf{h}_{AI}) z(i) + n_K(i), & \mathcal{H}_1 \end{cases} \quad (7)$$

where $n_K(i)$ represents the AWGN at Kevin.

Based on Kevin's observation of the received signals with vector $\mathbf{y}_K = [y_K(1), y_K(2), \dots, y_K(L)]$, He can decide whether or not Carol should transmit messages at each time slot. Since each element of \mathbf{y}_K is independent and identically distributed, each $y_K(i)$ obeys the following distribution:

$$\begin{cases} \mathcal{CN} \left(0, P_A |h_{AK} + \mathbf{h}_{IK}^T \Theta \mathbf{h}_{AI}|^2 + \sigma_K^2 \right), & \mathcal{H}_0 \\ \mathcal{CN} \left(0, P_C |h_{CK} + \mathbf{h}_{IK}^T \Theta \mathbf{h}_{CI}|^2 \right. \\ \quad \left. + P_A |h_{AK} + \mathbf{h}_{IK}^T \Theta \mathbf{h}_{AI}|^2 + \sigma_K^2 \right), & \mathcal{H}_1 \end{cases} \quad (8)$$

where σ_K^2 represents the noise variance at Kevin. Thus, the average received signal power Q at Kevin can be expressed as

$$Q = \begin{cases} P_A |h_{AK} + \mathbf{h}_{IK}^T \Theta \mathbf{h}_{AI}|^2 + \sigma_K^2, & \mathcal{H}_0 \\ P_A |h_{AK} + \mathbf{h}_{IK}^T \Theta \mathbf{h}_{AI}|^2 + \\ P_C |h_{CK} + \mathbf{h}_{IK}^T \Theta \mathbf{h}_{CI}|^2 + \sigma_K^2, & \mathcal{H}_1 \end{cases} \quad (9)$$

A radiometer is adopted as Kevin's detector [53] [54] [23], and then the decision rule at Kevin is expressed as

$$Q \underset{\mathcal{D}_0}{\overset{\mathcal{D}_1}{>}} \underset{\mathcal{D}_0}{<} \gamma, \quad (10)$$

where \mathcal{D}_1 and \mathcal{D}_0 represent that Carol transmits message or not, respectively. γ is a threshold value.

We use P_{FA} to represent the false alarm probability (i.e., $P\{\mathcal{D}_1 | \mathcal{H}_0\}$) that Carol did not transmit, but Kevin judged that he was transmitting. We use P_{MD} to denote the missed detection probability (i.e., $P\{\mathcal{D}_0 | \mathcal{H}_1\}$) that Carol conducted transmission, but Kevin judged that he did not transmit. Then, the detection error probability ξ at Kevin can be determined as

$$\xi = P_{FA} + P_{MD}. \quad (11)$$

Then, we say that Carol can achieve covert communications if $\xi \geq 1 - \varepsilon$ for any small $\varepsilon > 0$. From Kevin's perspective, he needs to conduct an optimal selection of γ to reach the minimum value ξ^* of ξ .

B. Probabilities of False Alarm and Missed Detection

Lemma 1. The false alarm probability P_{FA} is determined as:

$$P_{FA} = \begin{cases} \exp \left[-\frac{2(\gamma - \sigma_K^2)}{P_A \lambda_{AK}} \right], & \gamma > \sigma_K^2, \\ 1, & \text{otherwise.} \end{cases} \quad (12)$$

The missed detection probability P_{MD} follows:

$$P_{MD} = \begin{cases} 0, & \gamma < \sigma_K^2, \\ \frac{2}{\lambda_{CK}} \left[1 - \frac{2}{\lambda_{AK}} \cdot Ei \left(-\frac{\gamma - \sigma_K^2}{P_A \lambda_{AK}} \right) \right], & \sigma_K^2 < \gamma < \mathcal{V} + \sigma_K^2, \\ 1, & \text{otherwise.} \end{cases} \quad (13)$$

where $\mathcal{V} = |\mathbf{h}_{IK}^T \Theta \mathbf{h}_{AI} + h_{AK}|^2$, and Ei is the exponential integral function.

Proof: The detailed proof is provided in Appendix A. ■

C. The Optimal Detection Threshold of Kevin

To achieve the minimization of the detection error probability ξ defined in equation (11), Kevin has to select the threshold of his detector. Based on this optimal strategy for Kevin, we next derive the optimal detection threshold γ^* to minimize ξ .

$$\min_{\gamma} \quad \xi = P_{FA} + P_{MD}. \quad (14)$$

Lemma 2. *The optimal detection threshold γ^* of Kevin is determined as*

$$\gamma^* = \sigma_K^2 - P_A \lambda_{AK} \ln \left(\frac{2}{\lambda_{CK}} \right). \quad (15)$$

Proof: The detailed proof is provided in Appendix B. ■

V. TRANSMISSION OUTAGE ANALYSIS

This section first calculates the transmission outage probabilities from Carol to Ethan, which relies solely on the reflection path aided by an IRS due to obstacles, and from Alex to BS, which includes both direct and reflection paths.

A. Transmission Outage Probability from Carol to Ethan

Lemma 3. *We use δ_E to denote the transmission outage probability from Carol to Ethan. Then*

$$\delta_E = 1 - \frac{P_C \lambda_{AE} \exp \left(-\frac{\lambda_{CE} \gamma_E \sigma_E^2}{2P_C} \right)}{P_C \lambda_{AE} + \lambda_{CE} \gamma_E P_A}, \quad (16)$$

where $\gamma_E = 2^{R_{CE}} - 1$.

Proof: The detailed proof is provided in Appendix C. ■

B. Transmission Outage Probability from Alex to BS

Lemma 4. *We use δ_B to denote the transmission outage probability from Alex to BS. Then,*

$$\delta_B = 1 - \frac{P_C \lambda_{AB} \exp \left(-\frac{\lambda_{CB} \gamma_B \sigma_B^2}{2P_C} \right)}{P_C \lambda_{AB} + \lambda_{CB} \gamma_B P_A}, \quad (17)$$

where $\gamma_B = 2^{R_{AB}} - 1$.

Proof: The detailed proof is provided in Appendix D. ■

VI. COVERT RATE ANALYSIS

A. Formulation of the Optimization Problem

Our objective is to maximize the covert rate by jointly optimizing the transmission powers of Carol and Alex, and the IRS's reflection coefficient. To this end, the optimization problem is given by

$$\mathbf{P1} \quad \max_{P_C, P_A, \Theta} \quad R_{CE} (1 - \delta_E) \quad (18a)$$

$$\text{s.t.} \quad \xi^* \geq 1 - \varepsilon, \quad (18b)$$

$$\delta_B \leq \delta_{\max}, \quad (18c)$$

$$0 \leq q_n \leq 1, \forall n = 1, 2, \dots, N, \quad (18d)$$

$$0 \leq \theta_n \leq 2\pi, \forall n = 1, 2, \dots, N, \quad (18e)$$

$$0 \leq P_C \leq P_{C \max}, \quad (18f)$$

$$0 \leq P_A \leq P_{A \max}, \quad (18g)$$

where, (18b) represent the constraint of the covert requirement, (18c) represents the constraint of the transmission outage probability from Alex to BS, (18d) and (18e) represent the constraints of the amplitudes and phase shifts of IRS's reflecting elements, respectively, and (18f) and (18g) represent the constraints of the maximum transmission powers of Carol and Alex, respectively. R_{CE} is a constant representing a desired covert rate value. Thus, we can maximize $R_{CE}(1-\delta_E)$ by minimizing δ_E .

Problem **P1** is feasible if and only if the transmission powers P_C and P_A , the power limits $P_{C \max}$ and $P_{A \max}$, and the IRS constraints $\{q_n, \theta_n\}$ allow for configurations that simultaneously satisfy the covert requirement $\xi^* \geq 1 - \varepsilon$ and the outage probability constraint $\delta_B \leq \delta_{\max}$.

B. Optimal IRS Configuration, Θ

In this subsection, we derive the optimal IRS coefficients by combining the phase analysis method [24], [36] with the Gradient Descent (GD) approach.

We express $|\mathbf{h}_{IE}\Theta\mathbf{h}_{CI}|^2$ as

$$\left| \sum_{n=1}^N |h_{IE_n}| |h_{CI_n}| q_n e^{j(\theta_n + \arg(h_{IE_n}) + \arg(h_{CI_n}))} \right|^2, \quad (19)$$

where $\arg(\cdot)$ represents the argument of the principal value.

In equation (19), we aim to determine the optimal IRS phase shifts θ_n^* to align the reflected signals from the IRS with the direct signal at the receiver, thereby maximizing the signal strength at Kevin. The optimal IRS phase shifts θ_n^* are given by:

$$\theta_n^* = -[\arg(h_{IE_n}) + \arg(h_{CI_n})]. \quad (20)$$

Substituting θ_n^* into equation (19) allows us to rewrite the expression as:

$$\left| \sum_{n=1}^N |h_{IE_n}| |h_{CI_n}| q_n \right|^2. \quad (21)$$

This design maximizes the squared magnitude of the combined signals by ensuring that all individual signal contributions are perfectly in phase, leading to constructive interference and enhanced signal strength at the receiver.

Although the phase analysis method provides a theoretically optimal solution, practical systems often encounter noise, interference, and other non-ideal conditions that may prevent this solution from being globally optimal. In such cases, Gradient Descent (GD) can be employed to further fine-tune the phase shifts. This hybrid approach offers a comprehensive optimization strategy, blending theoretical precision with practical robustness. The specific algorithm is detailed in Algorithm 1.

Algorithm 1 Hybrid Analytical-Gradient Descent Optimization Algorithm for IRS phase shift, θ

Input: $P_C, P_A, \mathbf{h}_{IE}, \mathbf{h}_{CI}$, initial \mathbf{q}, θ , learning rate η , threshold ϵ , max iterations \max_iter

Output: Optimized θ^*

```

1: Initialize:
2:    $\theta_n^{(0)} = -\arg(h_{IE_n}) - \arg(h_{CI_n}), \forall n$ 
3:    $k \leftarrow 0$ 
4: while  $k < \max\_iter$  do
5:   Compute gradient:  $g_n^{(k)} = \frac{\partial \delta_E(\theta^{(k)})}{\partial \theta_n^{(k)}}, \forall n$ 
6:   Update:  $\theta_n^{(k+1)} = \theta_n^{(k)} - \eta \cdot g_n^{(k)}, \forall n$ 
7:   if  $\|\theta^{(k+1)} - \theta^{(k)}\| < \epsilon$  then
8:     break
9:   end if
10:   $k \leftarrow k + 1$ 
11: end while
12: return  $\theta^* = \theta^{(k)}$ 

```

Since in the optimization problem **P1**, the objective function in (18b) has R_{CE} as a preset constant, maximizing $R_{CE}(1 - \delta_E)$ can be transformed into minimizing δ_E . Thus, the optimization problem **P1** is reduced to **P1.1**.

$$\mathbf{P1.1} \quad \min_{P_C, P_A, \mathbf{q}} \delta_E(P_C, P_A, \mathbf{q}) \quad (22a)$$

$$\text{s.t.} \quad \xi^* \geq 1 - \epsilon, \quad (22b)$$

$$\delta_B \leq \delta_{\max}, \quad (22c)$$

$$0 \leq q_n \leq 1, \forall n = 1, 2, \dots, N, \quad (22d)$$

$$0 \leq P_C \leq P_{C\max}, \quad (22e)$$

$$0 \leq P_A \leq P_{A\max}, \quad (22f)$$

where, the expression for δ_E is given in (16) of Lemma 3. The reflection amplitude vector of reflecting elements \mathbf{q} is represented as $[q_1, q_2, \dots, q_N]^T$.

C. Optimal transmission power of the D2D Transmitter Carol, P_C

We first determine the monotonicity of δ_E with respect to P_C and find:

$$\frac{\partial \delta_E}{\partial P_C} = -\frac{\lambda_{AE}^2 \lambda_{CE} \gamma_E \exp\left[\left(\frac{P_A - \sigma_K^2}{2}\right) \frac{\lambda_{CE} \gamma_E \sigma_E^2}{2P_C}\right]}{(P_C \lambda_{AE} + \lambda_{CE} \gamma_E P_A)^2}. \quad (23)$$

Since (23) is less than zero, δ_E is a monotonically decreasing function of P_C . Therefore, to find the optimal P_C , denoted as P_C^* , within the interval $0 \leq P_C \leq P_{C\max}$ while ensuring the constraint $\xi^* \geq 1 - \epsilon$ is satisfied, we should identify the largest value of P_C that meets this constraint and maximizes performance.

From Lemma 2, we have:

$$\begin{aligned} \xi^* &= \exp\left(-\frac{\gamma^* - \sigma_K^2}{P_A \lambda_{AK}}\right) + 1 - \frac{\exp\left(-\frac{\gamma^* - \sigma_K^2}{P_C \lambda_{CK}}\right)}{\lambda_{AK} - \frac{P_A}{P_C \lambda_{CK}}} \\ &\geq 1 - \epsilon. \end{aligned} \quad (24)$$

Rearranging the constraint:

$$1 - \frac{\exp\left(-\frac{\gamma^* - \sigma_K^2}{P_C \lambda_{CK}}\right)}{\lambda_{AK} - \frac{P_A}{P_C \lambda_{CK}}} \geq 1 - \epsilon - \exp\left(-\frac{\gamma^* - \sigma_K^2}{P_A \lambda_{AK}}\right). \quad (25)$$

Simplifying gives:

$$\frac{\exp\left(-\frac{\gamma^* - \sigma_K^2}{P_C \lambda_{CK}}\right)}{\lambda_{AK} - \frac{P_A}{P_C \lambda_{CK}}} \leq \epsilon - \exp\left(-\frac{\gamma^* - \sigma_K^2}{P_A \lambda_{AK}}\right). \quad (26)$$

Let $\Delta = \epsilon - \exp\left(-\frac{\gamma^* - \sigma_K^2}{P_A \lambda_{AK}}\right)$.
So the constraint becomes:

$$\frac{\gamma^* - \sigma_K^2}{P_C} \geq -\lambda_{CK} \ln\left(\Delta \left(\lambda_{AK} - \frac{P_A}{P_C \lambda_{CK}}\right)\right). \quad (27)$$

Isolating P_C , we get:

$$P_C \leq \frac{\gamma^* - \sigma_K^2}{-\lambda_{CK} \ln\left(\Delta \lambda_{AK} - \frac{\Delta P_A}{P_C \lambda_{CK}}\right)}. \quad (28)$$

Thus, the optimal P_C is:

$$P_C^* = \max\left(P_{C\max}, \frac{\gamma^* - \sigma_K^2}{-\lambda_{CK} \ln\left(\Delta \lambda_{AK} - \frac{\Delta P_A}{P_C \lambda_{CK}}\right)}\right). \quad (29)$$

D. Optimal Transmission Power of Cellular User Alex, P_A

To determine the monotonicity of δ_E with respect to P_A , we compute the partial derivative of (16) with respect to P_A and obtain:

$$\frac{\partial \delta_E}{\partial P_A} = \frac{P_C \lambda_{AE} \exp\left(-\frac{\lambda_{CE} \gamma_E \sigma_E^2}{2P_C}\right) \cdot \lambda_{CE} \gamma_E}{(P_C \lambda_{AE} + \lambda_{CE} \gamma_E P_A)^2}. \quad (30)$$

Thus, the objective function of **P1.1** is a monotonically increasing function of P_A . This implies that to minimize δ_E , P_A should be set to its minimum value, subject to the constraints given in (22b), (22c), and (22e).

For constraint (22b), we derive the monotonicity of ξ^* with respect to P_A by taking the partial derivative of ξ^* in the interval $\sigma_K^2 < \gamma < \mathcal{V} + \sigma_K^2$. We have:

$$\begin{aligned} \frac{\partial \xi^*}{\partial P_A} &= \exp\left(-\frac{\gamma^* - \sigma_K^2}{P_A \lambda_{AK}}\right) \cdot \frac{\gamma^* - \sigma_K^2}{P_A^2 \lambda_{AK}} \\ &\quad + \frac{\exp\left(-\frac{\gamma^* - \sigma_K^2}{P_C \lambda_{CK}}\right)}{\left(\lambda_{AK} - \frac{P_A}{P_C \lambda_{CK}}\right)^2} \cdot \frac{1}{P_C \lambda_{CK}} > 0. \end{aligned} \quad (31)$$

Thus, ξ^* is an increasing function of P_A . The minimum optimal value of P_A , denoted as P_A^{1*} , must satisfy the condition:

$$\xi^*(P_A^{1*}) = 1 - \epsilon. \quad (32)$$

We cannot obtain a closed form of P_A^{1*} because P_A^{1*} appears in both the regular and exponential terms. However, it can be determined using numerical methods such as the Newton-Raphson method.

Meanwhile, P_A must also satisfy the constraint in (22c) to ensure non-outage transmission from Alex to the BS. Next, we analyze the monotonicity of δ_B with respect to P_A . To analyze this, we compute the partial derivatives of β with respect to P_A and δ_B with respect to β , and obtain:

$$\frac{\partial \beta}{\partial P_A} = -\lambda_{AB} \frac{2^{R_{AB}} - 1}{P_A^2} < 0, \quad (33)$$

and

$$\frac{\partial \delta_B}{\partial \beta} = \frac{\lambda_{CB} \exp(-\beta \sigma_B^2) (\sigma_B^2 (\lambda_{CB} + \beta P_C) + P_C)}{(\lambda_{CB} + \beta P_C)^2} > 0. \quad (34)$$

Thus, β decreases with increasing P_A and δ_B increases with increasing β , so δ_B is a decreasing function of P_A .

We can then determine another minimum optimal value of P_A , denoted as P_A^{2*} , which must satisfy the condition:

$$\delta_B(P_A^{2*}) = \delta_{\max}. \quad (35)$$

Substituting (17) into (35), P_A^{2*} can be determined as:

$$P_A^{2*} = \lambda_{AB} \sigma_B^2 (2^{R_{AB}} - 1) \cdot \text{LamW}^{-1} \left[\frac{\lambda_{CB} \sigma_B^2 (P_C^* + \lambda_{CB})}{1 - \delta_{\max}} \right], \quad (36)$$

where LamW is the Lambert W-function, defined as the function W satisfying the equation $W \exp(W) = x$.

Considering the above analysis and the non-negativity constraint (22e), the optimal P_A^* is given by:

$$P_A^* = \min\{P_A^{1*}, P_A^{2*}, 0\}. \quad (37)$$

The above solution process is summarized in Algorithm 2.

Algorithm 2 Optimal Transmission Power for Cellular User Alex, P_A^*

Input: $R_{AB}, \delta_{\max}, \sigma_B^2, \lambda_{AB}, \lambda_{CK}, \gamma^*, \sigma_K^2, P_C^*$

Output: Optimal transmission power P_A^*

- 1: **Step 1:** Compute $P_A^{(1)*}$ by solving equation (32).
 - 2: **Step 2:** Compute $P_A^{(2)*}$ by solving equation (36).
 - 3: **Step 3:** Determine final optimal power P_A^* using equation (37).
 - 4: **return** P_A^*
-

E. Optimal IRS Reflection Amplitude Vector, \mathbf{q}

To determine the optimal \mathbf{q} , we use a one-dimensional search method [21]. Let A represent the received power at Kevin from Carol. Since ξ^* is always a decreasing function of A , we rewrite (22b) as $A \leq L(\varepsilon)$ for a given η to ensure $\xi^* \geq 1 - \varepsilon$, where $L(\eta)$ is the upper bound of A .

Then, the optimization problem in **P1.1** is reduced to **P1.2**:

$$\mathbf{P1.2} \quad \min_{P_C^*, P_A^*, \mathbf{q}} \delta_E(P_C^*, P_A^*, \mathbf{q}) \quad (38a)$$

$$\text{s.t.} \quad A \leq L(\eta), \quad (38b)$$

$$\delta_B \leq \delta_{\max}, \quad (38c)$$

$$0 \leq q_n \leq 1, \forall n = 1, 2, \dots, N. \quad (38d)$$

Since both the objective function (38a) and the covert-ness constraint (38b) are non-convex, the optimization problem **P1.2** is non-convex. It can be transformed into a convex optimization problem by reformulating equation (21) as $\mathbf{q}^T \mathbf{H}_I$ and transforming constraint (38b) into $\sigma_K^2 (P_C^* \mathbf{q})^T \mathbf{T}_{CI} (P_C^* \mathbf{q}) \leq L(\eta)$. Here, $\mathbf{H}_I = [|h_{IE_1}| |h_{CI_1}|, |h_{IE_2}| |h_{CI_2}|, \dots, |h_{IE_n}| |h_{CI_n}|]^T$ and $\mathbf{T}_{CI} = \text{diag}\{|h_{CI_1}|^2, |h_{CI_2}|^2, \dots, |h_{CI_n}|^2\}$. We use a MATLAB-based modeling system (such as CVX) to solve this convex optimization problem [55] [56].

So far, we have analyzed the optimization of P_C , P_A , and Θ . Next, we present the iterative hybrid analytical-gradient descent optimization algorithm 3, designed to avoid local optima and achieve more accurate results.

Algorithm 3 Iterative Covert Rate Optimization

Input: P_C^{\max}, P_A^{\max} , initial \mathbf{q}, θ , learning rate η , threshold ε , max iterations max_iter

Output: Optimized $\theta^*, P_C^*, P_A^*, \mathbf{q}^*$

- 1: Initialize $k = 0$
 - 2: Set $\theta_n^{(0)} = -[\arg(h_{IE_n}) + \arg(h_{CI_n})], \forall n$
 - 3: Initialize $P_C^{(0)}, P_A^{(0)}, \mathbf{q}^{(0)}$
 - 4: **repeat**
 - 5: **Step 1:** Update $\theta_n^{(k+1)} = \theta_n^{(k)} - \eta \cdot g_n^{(k)}$
 - 6: **Step 2:** Update $P_C^{(k+1)}$ via closed-form
 - 7: **Step 3:** Compute $P_A^{(k+1)} = \min\{P_A^{1*}, P_A^{2*}, 0\}$
 - 8: **Step 4:** Update $\mathbf{q}^{(k+1)}$ via 1D search to satisfy $A \leq L(\eta)$
 - 9: **Step 5:** Check convergence:
 - 10: **if** $\|\theta^{(k+1)} - \theta^{(k)}\| < \varepsilon$ **and** similar for \mathbf{q}, P_C, P_A **then**
 - 11: **break**
 - 12: **end if**
 - 13: $k \leftarrow k + 1$
 - 14: **until** $k \geq \text{max_iter}$
 - 15: **return** $\theta^*, P_C^*, P_A^*, \mathbf{q}^*$
-

VII. NUMERICAL RESULTS

This section conducts a simulation study to illustrate how system parameters affect the covert rate performance. The system parameters used in this simulation are listed in TABLE II. We propose two sets of Rician K -factors for simulation. Set 1 aims to maximize the covert D2D rate, particularly for Carol-to-Ethan communication. It assigns a high K_{IE} value (15 dB) to ensure strong LoS between the IRS and Ethan, thereby enhancing covert signal delivery. K_{CI} is set to a moderate-to-high value (8 dB) to support the primary D2D transmission path while maintaining acceptable interference levels. Meanwhile, K_{AI} is kept moderate (6 dB) to balance cellular benefits and avoid excessive interference with Ethan, and K_{IK} remains low (1 dB) to suppress signal leakage to Kevin for better covertness. Set 2 emphasizes a balanced enhancement of overall D2D-enabled cellular performance. It increases K_{AI} to 10 dB and K_{IB} to 12 dB, thereby improving IRS-assisted cellular transmission. Although K_{IE} and K_{CI} remain relatively high (13 dB and 5 dB, respectively), they

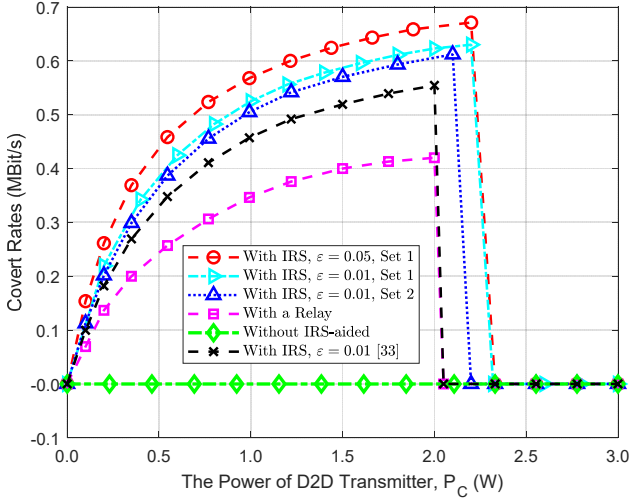


Fig. 2. Covert rates versus the power of D2D transmitter Carol

are slightly reduced compared to Set 1, resulting in a moderately strong D2D rate. K_{IK} is set slightly higher at 2 dB, allowing limited IRS influence on Kevin without significantly compromising covert communication. This comparison highlights the inherent trade-off between maximizing D2D covert communication and enhancing cellular performance in IRS-assisted Rician channels.

TABLE II
SYSTEM PARAMETERS

System parameters	Values
Maximum transmission powers of Carol and Alex ($P_{C \max}, P_{A \max}$)	1.0 W
Noise variance at Ethan, BS, and Kevin ($\sigma_E^2, \sigma_B^2, \sigma_K^2$)	0.01 W
Noise variances over channel \mathbf{h}_{XY} (σ_{XY}^2)	0.005 W
Pre-determined rates for \mathbf{h}_{CE} and \mathbf{h}_{AB} (R_{CE}, R_{AB})	1 Mbit/s
Covertiness requirement (ϵ)	0.01
K -factor for IRS related channels ($K_{AI}, K_{CI}, K_{IE}, K_{IB}, K_{IK}$)	Set 1: 6, 8, 15, 10, 1 Set 2: 10, 5, 13, 12, 2

A. Covert Rate

Figure 2 illustrates the impact of Carol's transmission power, P_C , on the covert rates across different scenarios: *With IRS*, $\epsilon = 0.05$ (*Set 1*); *With IRS*, $\epsilon = 0.01$ (*Set 1*); *With IRS*, $\epsilon = 0.01$ (*Set 2*); *With a Relay*; *Without IRS-aided*; and *With IRS*, $\epsilon = 0.01$ (as referenced in [33]).

In scenarios without IRS or relay assistance, the covert rate remains consistently zero due to obstacles that completely block the transmission from Carol to Ethan. In the scenarios aided by IRS, the covert rates initially increase as P_C rises because the signal strength received by Ethan improves, leading to a higher covert rate. However, this trend only continues up to a certain point. Once P_C exceeds a critical threshold, the transmission becomes strong enough to be detected by the warden, Kevin. At this point, the covertiness constraint is violated, and the covert rate drops to zero. This threshold represents the maximum transmission power that Carol can use while still

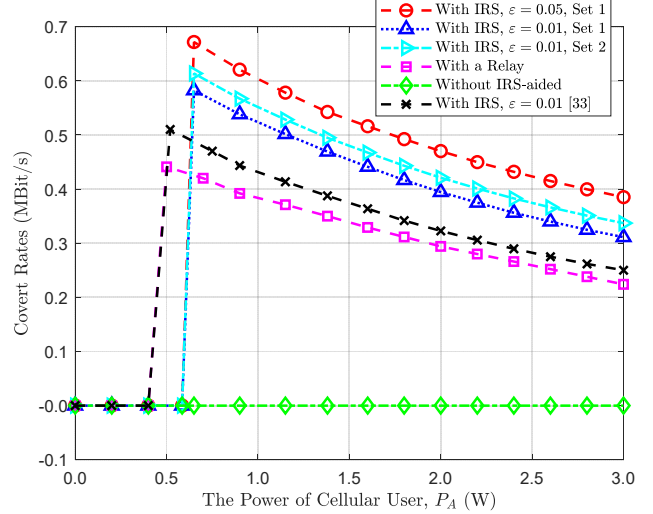


Fig. 3. Covert rates versus the power of cellular user Alex

maintaining undetectable communication. If the power exceeds this threshold, Kevin can detect the transmission, resulting in the failure of covert communication.

Additionally, the scenarios with different values of ϵ , which adjust the strictness of the covertiness constraint, show that a higher ϵ relaxes this constraint, permitting a higher covert rate before the threshold is reached. This means that Carol can transmit at a higher power without being detected, as the system tolerates a slightly higher probability of detection.

The scenario with relay assistance shows an increase in covert rate, but it reaches a lower peak compared to the IRS scenarios before leveling off. This trend results from the relay's ability to amplify and retransmit signals, providing a boost to the signal strength received by Ethan. However, the relay's amplification is less effective than the IRS's reflection and beamforming capabilities. As P_C continues to increase, the relay scenario reaches a plateau and does not achieve the same maximum covert rate as the IRS. This is because the relay amplifies noise and interference along with the signal, limiting its overall effectiveness. Ultimately, while the relay improves the covert rate compared to the no-assistance scenario, its performance is consistently lower than that of the IRS-aided scenarios.

Among the IRS-aided configurations, *Set 1* achieves higher covert rates than *Set 2* under identical conditions, primarily due to its Rician K -factor configuration that prioritizes covert D2D links. In contrast, *Set 2* embodies a trade-off between maximizing covert communication and enhancing overall cellular performance in IRS-assisted systems. The subsequent simulation results reflect the same design rationale.

Fig. 3 illustrates the impact of cellular user Alex's transmission power, P_A , on the covert rates under various scenarios: *with IRS*, *with a relay*, *without any aid*, and *using the method in [32]*. In the scenario without IRS or relay assistance, the covert rate remains at zero as P_A increases because the direct transmission from Alex to the base station is completely blocked by obstacles. In the IRS-aided scenario, the covert rate initially stays at zero when P_A is low due to communication

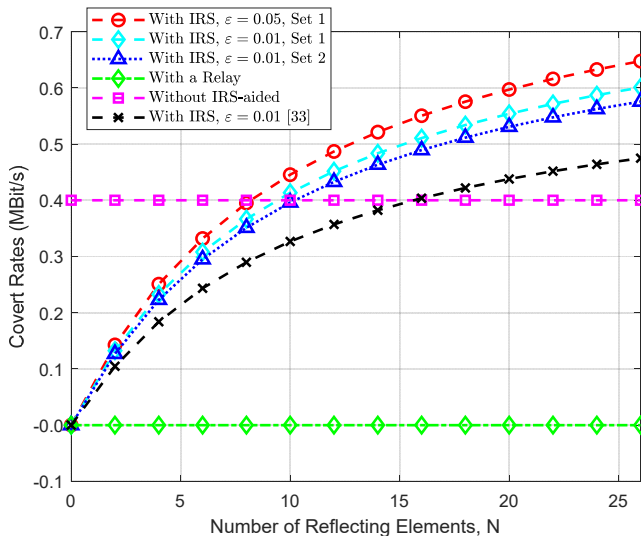


Fig. 4. Covert rates versus number of reflecting elements, N

outages. As P_A increases, the IRS enhances the signal through reflection and beamforming, enabling a non-zero covert rate. This rate continues to rise until P_A reaches a critical threshold, beyond which the increased power leads to higher interference at Ethan, which the IRS cannot fully mitigate. Consequently, the covert rate starts to decline as the IRS's ability to optimize signal reflection and maintain covertness becomes limited. In the scenario with relay assistance, the covert rate also starts at zero but achieves a non-zero value more quickly due to the relay's active signal amplification. The relay allows the covert rate to increase rapidly but it plateaus at a lower level compared to the IRS because the relay lacks the IRS's precision in optimizing signal direction. As P_A continues to increase, the relay's amplification of both the desired signal and the accompanying noise and interference leads to a gradual decrease in the covert rate. However, this decline is smoother than with the IRS, owing to the relay's more consistent amplification capabilities. Ultimately, the IRS demonstrates superior performance in optimizing the covert rate by intelligently reflecting and directing signals, achieving a higher peak covert rate. The key thresholds in both the IRS and relay scenarios highlight the delicate balance between enhancing signal strength and maintaining covertness. In the IRS scenario, the covert rate declines more sharply beyond the threshold due to the IRS's limited capacity to control interference, whereas the relay's performance declines more gradually but at a lower overall covert rate.

Fig. 4 shows the impact of the number of reflecting elements N on the covert rates under different scenarios, including with IRS, without IRS, with a relay, and using the method in [32]. We can see from Fig. 4 that as N increases, the covert rate increases with each IRS-aided scenario while it remains at zero without an IRS-aided scenario. This is because increasing the number of reflecting elements N enhances the reflection performance of the IRS, thereby improving covert rate performance in IRS-aided scenarios. In contrast, the scenario that assisted by a relay maintains a constant

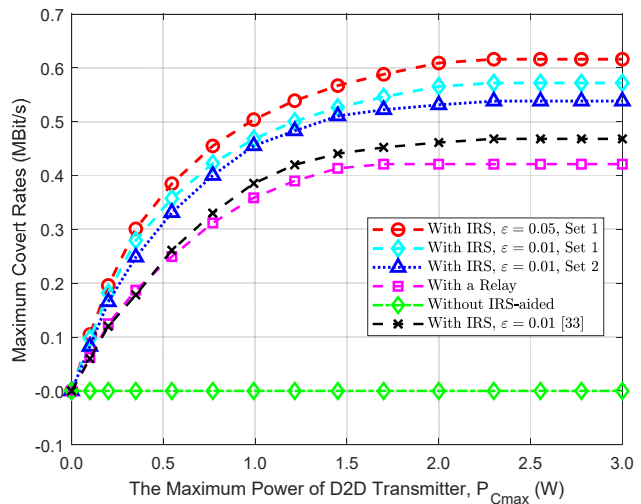


Fig. 5. Maximum covert rates versus the maximum power of D2D transmitter Carol

covert rate regardless of N . This is because the relay operates independently of the IRS and provides a steady covert rate through active signal amplification, unaffected by changes in the number of reflecting elements.

B. Maximum Covert Rate

Fig. 5 explores the impact of the maximum transmission power $P_{C\max}$ of the D2D covert transmitter Carol on the maximum covert rates under different scenarios. We can see from Fig. 5 that as $P_{C\max}$ increases, the maximum covert rate first increases and then remains unchanged with each IRS-aided scenario, while it remains at zero without an IRS-aided scenario. This phenomenon occurs because an increase in the transmission power P_C can improve the covert rate performance from Carol to Ethan and also increase the transmission outage probability from Alex to BS. Thus, there exists an optimal transmission power P_C to maximize the covert rate. As $P_{C\max}$ is relatively small, P_C cannot reach the optimal value, and thus the covert rate increases with $P_{C\max}$. As $P_{C\max}$ continues to increase, P_C reaches the optimal value, and thus the maximum covert rate remains unchanged. Without an IRS-aided scenario, the reason is the same as that in Fig. 2.

In the scenario with a relay, the maximum covert rate initially increases as $P_{C\max}$ grows, but the increase is more gradual compared to IRS scenarios. This is because the relay provides active amplification of signals but lacks the reflective optimization that IRS offers. IRS technology leverages its ability to intelligently reflect signals towards desired paths and adjust phases to minimize interference and maximize signal strength at the receiver, thus enhancing the covert rate more efficiently. In contrast, a relay amplifies both the desired signal and noise, which can introduce additional interference, reducing its effectiveness. Consequently, the covert rate with a relay plateaus at a lower value than with IRS. The relay is effective in boosting signal strength but does not match the precise signal control and efficiency provided by IRS,

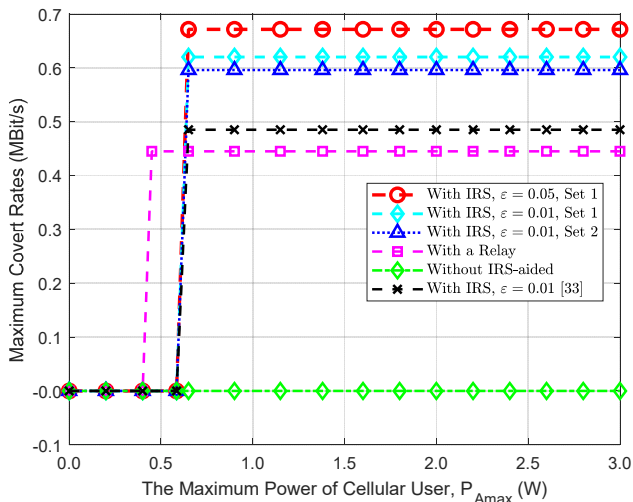


Fig. 6. Maximum covert rates versus the maximum power of the cellular user, Alex

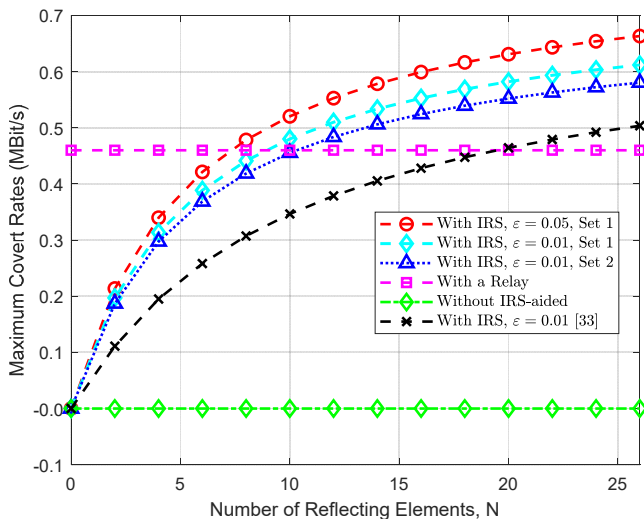


Fig. 7. Maximum covert rates versus number of reflecting elements, N

which results in a lower optimal covert rate level. As with the IRS scenarios, the covert rate reaches a steady state once P_C achieves its optimal value, illustrating the relay's limited capability to further enhance the covert rate beyond this point.

Fig. 6 depicts how the maximum covert rates vary with the maximum power of cellular user Alex, P_A , under different scenarios. We observe from Fig. 6 that when $P_{A\max}$ increases, the maximum covert rate without an IRS-aided scenario keeps at zero, which is due to the fact that the transmission from Carol to Ethan is completely blocked by obstacles. We also observe that as $P_{A\max}$ increases, the maximum covert rate under each IRS-aided scenario first stays at zero, then increases up to a constant and keeps unchanged. It can be explained as follows. When $P_{A\max}$ is relatively small, the constraint that the transmission from Alex to BS is not outage cannot be satisfied, and thus the maximum covert rate is zero. When $P_{A\max}$ further increases, the constraint is satisfied, and thus maximum covert rate reaches a maximum constant.

Fig. 7 explores how the maximum covert rates vary with the number of reflecting elements, N , under different scenarios. It can be observed from Fig. 7 that as N increases, the maximum covert rate without an IRS-aided scenario remains at zero, while it increases monotonically with each IRS-aided scenario. The maximum covert rate under each IRS-aided scenario improves as N increases because the additional reflecting elements enhance the IRS's ability to direct and focus the signal, thereby improving covert rate performance. In contrast, the scenario with relay assistance maintains a constant covert rate regardless of the number of reflecting elements. This is because the relay operates independently of the IRS and does not benefit from the increased reflection capability, instead providing a steady level of signal amplification.

VIII. CONCLUSION

This paper examined the covert communication of a D2D pair in an IRS-enabled D2D network. We derived fundamental results concerning detection error probability, optimal detection thresholds, and transmission outage probabilities. Based on these findings, we developed a theoretical model for covert rate and formulated its maximization as a constrained optimization problem. We achieved covert rate maximization through the joint optimization of the IRS reflection coefficients and the transmission powers of both the cellular user and the D2D transmitter. Numerical results demonstrate that the IRS can significantly enhance covert rate performance.

Future studies will emphasize practical implementations on real hardware, addressing the imperfections and challenges associated with IRS technology. Furthermore, building upon foundational efforts in areas such as inter-UAV collision avoidance, efficient resource allocation, and advanced handover algorithms will be essential for managing the growing complexity and demands of covert communication systems [57]–[59]. In addition, incorporating a multi-antenna BS into covert communications within IRS-assisted Vehicle-to-Everything (V2X) networks, combined with, matrix-based analysis, and DRL-driven joint beamforming, represents a promising direction for future research.

REFERENCES

- [1] D. Shi, L. Li, T. Ohtsuki, M. Pan, Z. Han, and H. V. Poor, "Make Smart Decisions Faster: Deciding D2D Resource Allocation via Stackelberg Game Guided Multi-Agent Deep Reinforcement Learning," *IEEE Transactions on Mobile Computing*, vol. 21, no. 12, pp. 4426–4438, 2022.
- [2] R. Amer, H. ElSawy, J. Kibilda, M. M. Butt, and N. Marchetti, "Performance Analysis and Optimization of Cache-Assisted CoMP for Clustered D2D Networks," *IEEE Transactions on Mobile Computing*, vol. 21, no. 4, pp. 1334–1348, 2022.
- [3] I. Budhiraja, N. Kumar, and S. Tyagi, "ISHU: Interference Reduction Scheme for D2D Mobile Groups Using Uplink NOMA," *IEEE Transactions on Mobile Computing*, vol. 21, no. 9, pp. 3208–3224, 2022.
- [4] Z. Xiao, J. Shu, H. Jiang, J. C. S. Lui, G. Min, J. Liu, and S. Dustdar, "Multi-Objective Parallel Task Offloading and Content Caching in D2D-Aided MEC Networks," *IEEE Transactions on Mobile Computing*, vol. 22, no. 11, pp. 6599–6615, 2023.
- [5] M. Zhang, B. Yang, S. Zhao, and L. Ma, "Secrecy Capacity Analysis in D2D-Enabled Cellular Networks Under Power Control," in *2019 International Conference on Networking and Network Applications (NaNA)*, 2019, pp. 81–84.

- [6] Z. Li, J. Wang, S. Long, J. Fu, M. Yang, and J. Weng, "A Trust Evaluation Joint Active Detection Method in Video Sharing D2D Networks," *IEEE Transactions on Mobile Computing*, pp. 1–14, 2023.
- [7] W. Gao, Y. Chen, C. Han, and Z. Chen, "Distance-Adaptive Absorption Peak Modulation (DA-APM) for Terahertz Covert Communications," *IEEE Transactions on Wireless Communications*, vol. 20, no. 3, pp. 2064–2077, 2021.
- [8] B. A. Bash, D. Goeckel, and D. Towsley, "Limits of Reliable Communication with Low Probability of Detection on AWGN Channels," *IEEE Journal on Selected Areas in Communications*, vol. 31, no. 9, pp. 1921–1930, 2013.
- [9] P. H. Che, M. Bakshi, and S. Jaggi, "Reliable deniable communication: Hiding messages in noise," in *2013 IEEE International Symposium on Information Theory*, 2013, pp. 2945–2949.
- [10] L. Wang, G. W. Wornell, and L. Zheng, "Fundamental Limits of Communication With Low Probability of Detection," *IEEE Transactions on Information Theory*, vol. 62, no. 6, pp. 3493–3503, 2016.
- [11] K. Shahzad and X. Zhou, "Covert Wireless Communications Under Quasi-Static Fading With Channel Uncertainty," *IEEE Transactions on Information Forensics and Security*, vol. 16, pp. 1104–1116, 2021.
- [12] K. Shahzad, X. Zhou, and S. Yan, "Covert Communication in Fading Channels under Channel Uncertainty," in *2017 IEEE 85th Vehicular Technology Conference (VTC Spring)*, 2017, pp. 1–5.
- [13] A. Sheikholeslami, M. Ghaderi, and D. Goeckel, "Covert Communications in Multi-Channel Slotted ALOHA Systems," *IEEE Transactions on Mobile Computing*, vol. 21, no. 6, pp. 1958–1971, 2022.
- [14] Y. Su, H. Sun, Z. Zhang, Z. Lian, Z. Xie, and Y. Wang, "Covert Communication With Relay Selection," *IEEE Wireless Communications Letters*, vol. 10, no. 2, pp. 421–425, 2021.
- [15] J. Hu, S. Yan, F. Shu, and J. Wang, "Covert Transmission With a Self-Sustained Relay," *IEEE Transactions on Wireless Communications*, vol. 18, no. 8, pp. 4089–4102, 2019.
- [16] J. Hu, S. Yan, X. Zhou, F. Shu, J. Li, and J. Wang, "Covert Communication Achieved by a Greedy Relay in Wireless Networks," *IEEE Transactions on Wireless Communications*, vol. 17, no. 7, pp. 4766–4779, 2018.
- [17] C. Gao, B. Yang, X. Jiang, H. Inamura, and M. Fukushi, "Covert Communication in Relay-Assisted IoT Systems," *IEEE Internet of Things Journal*, vol. 8, no. 8, pp. 6313–6323, 2021.
- [18] A. Sheikholeslami, M. Ghaderi, D. Towsley, B. A. Bash, S. Guha, and D. Goeckel, "Multi-Hop Routing in Covert Wireless Networks," *IEEE Transactions on Wireless Communications*, vol. 17, no. 6, pp. 3656–3669, 2018.
- [19] Q. T. Ngo, B. A. Jayawickrama, Y. He, and E. Dutkiewicz, "Multi-agent drl-based ris-assisted spectrum sensing in cognitive satellite-terrestrial networks," *IEEE Wireless Communications Letters*, vol. 12, no. 12, pp. 2213–2217, 2023.
- [20] Q. Wu and R. Zhang, "Towards Smart and Reconfigurable Environment: Intelligent Reflecting Surface Aided Wireless Network," *IEEE Communications Magazine*, vol. 58, no. 1, pp. 106–112, 2020.
- [21] C. Wu, S. Yan, X. Zhou, R. Chen, and J. Sun, "Intelligent Reflecting Surface (IRS)-Aided Covert Communication with Warden's Statistical CSI," *IEEE Wireless Communications Letters*, vol. 10, no. 7, pp. 1449–1453, 2021.
- [22] J. Si, Z. Li, Y. Zhao, J. Cheng, L. Guan, J. Shi, and N. Al-Dhahir, "Covert Transmission Assisted by Intelligent Reflecting Surface," *IEEE Transactions on Communications*, vol. 69, no. 8, pp. 5394–5408, 2021.
- [23] C. Wang, Z. Li, J. Shi, and D. W. K. Ng, "Intelligent Reflecting Surface-Assisted Multi-Antenna Covert Communications: Joint Active and Passive Beamforming Optimization," *IEEE Transactions on Communications*, vol. 69, no. 6, pp. 3984–4000, 2021.
- [24] X. Zhou, S. Yan, Q. Wu, F. Shu, and D. W. K. Ng, "Intelligent Reflecting Surface (IRS)-Aided Covert Wireless Communications With Delay Constraint," *IEEE Transactions on Wireless Communications*, vol. 21, no. 1, pp. 532–547, 2022.
- [25] J. Kong, F. T. Dagefus, J. Choi, and P. Spasojevic, "Intelligent Reflecting Surface Assisted Covert Communication With Transmission Probability Optimization," *IEEE Wireless Communications Letters*, vol. 10, no. 8, pp. 1825–1829, 2021.
- [26] X. Chen, T.-X. Zheng, L. Dong, M. Lin, and J. Yuan, "Enhancing MIMO Covert Communications via Intelligent Reflecting Surface," *IEEE Wireless Communications Letters*, vol. 11, no. 1, pp. 33–37, 2022.
- [27] R. Sun, B. Yang, Y. Shen, X. Jiang, and T. Taleb, "Covert and Secrecy Study in Untrusted Relay-Assisted D2D Networks," *IEEE Internet of Things Journal*, vol. 10, no. 1, pp. 17–30, 2023.
- [28] J. Lee and J. H. Lee, "Performance Analysis and Resource Allocation for Cooperative D2D Communication in Cellular Networks With Multiple D2D Pairs," *IEEE Communications Letters*, vol. 23, no. 5, pp. 909–912, 2019.
- [29] R. M. Radaydeh, F. S. Al-Qahtani, A. Celik, K. A. Qaraqe, and M.-S. Alouini, "Generalized Imperfect D2D Associations in Spectrum-Shared Cellular Networks Under Transmit Power and Interference Constraints," *IEEE Access*, vol. 8, pp. 182517–182536, 2020.
- [30] D.-W. Lim, J. Kang, and H.-M. Kim, "Adaptive Power Control for D2D Communications in Downlink SWIPT Networks With Partial CSI," *IEEE Wireless Communications Letters*, vol. 8, no. 5, pp. 1333–1336, 2019.
- [31] G. Zhao, S. Chen, L. Qi, L. Zhao, and L. Hanzo, "Mobile-Traffic-Aware Offloading for Energy- and Spectral-Efficient Large-Scale D2D-Enabled Cellular Networks," *IEEE Transactions on Wireless Communications*, vol. 18, no. 6, pp. 3251–3264, 2019.
- [32] Y. Yang, S. Shen, Y. She, W. Wang, B. Yang, and Y. Gao, "On IRS-Aided Covert Communications of D2D-Enabled Cellular Networks," in *2022 International Conference on Networking and Network Applications (NaNA)*, 2022, pp. 1–6.
- [33] A. Abdelaziz and C. E. Koksal, "Fundamental limits of covert communication over MIMO AWGN channel," in *2017 IEEE Conference on Communications and Network Security (CNS)*, 2017, pp. 1–9.
- [34] R. Soltani, D. Goeckel, D. Towsley, and A. Houmansadr, "Covert Communications on Poisson Packet Channels," in *2015 53rd Annual Allerton Conference on Communication, Control, and Computing (Allerton)*, 2015, pp. 1046–1052.
- [35] Y. Cheng, J. Lu, D. Niyato, B. Lyu, M. Xu, and S. Zhu, "Performance Analysis and Power Allocation for Covert Mobile Edge Computing With RIS-Aided NOMA," *IEEE Transactions on Mobile Computing*, pp. 1–16, 2023.
- [36] Y. Wu, X. Chen, M. Liu, L. Xu, N. Zhao, X. Wang, and D. W. K. Ng, "IRS-Assisted Covert Communication With Equal and Unequal Transmit Prior Probabilities," *IEEE Transactions on Communications*, vol. 72, no. 5, pp. 2897–2912, 2024.
- [37] X. Chen, Z. Chang, M. Liu, N. Zhao, T. Hämäläinen, and D. Niyato, "UAV-IRS Assisted Covert Communication: Introducing Uncertainty via Phase Shifting," *IEEE Wireless Communications Letters*, vol. 13, no. 1, pp. 103–107, 2024.
- [38] J. Kong, F. T. Dagefu, J. Choi, R. Aggarwal, and P. Spasojevic, "Covert Communication in Intelligent Reflecting Surface Assisted Networks With a Friendly Jammer," *IEEE Transactions on Vehicular Technology*, vol. 73, no. 1, pp. 1467–1472, 2024.
- [39] Z. Chen, S. Yan, X. Zhou, F. Shu, and D. W. K. Ng, "Intelligent Reflecting Surface-Assisted Passive Covert Wireless Detection," *IEEE Transactions on Vehicular Technology*, vol. 73, no. 2, pp. 2954–2959, 2024.
- [40] W. Wang, L. Yang, A. Meng, Y. Zhan, and D. W. K. Ng, "Resource Allocation for IRS-aided JP-CoMP Downlink Cellular Networks with Underlying D2D Communications," *IEEE Transactions on Wireless Communications*, pp. 1–1, 2021.
- [41] S. Mao, X. Chu, Q. Wu, L. Liu, and J. Feng, "Intelligent Reflecting Surface Enhanced D2D Cooperative Computing," *IEEE Wireless Communications Letters*, vol. 10, no. 7, pp. 1419–1423, 2021.
- [42] Y. Liu, Q. Hu, Y. Cai, and M. Juntti, "Latency Minimization in Intelligent Reflecting Surface Assisted D2D Offloading Systems," *IEEE Communications Letters*, vol. 25, no. 9, pp. 3046–3050, 2021.
- [43] C. Cai, H. Yang, X. Yuan, and Y.-C. Liang, "Two-Timescale Optimization for Intelligent Reflecting Surface Aided D2D Underlay Communication," in *GLOBECOM 2020 - 2020 IEEE Global Communications Conference*, 2020, pp. 1–6.
- [44] Z. Peng, T. Li, C. Pan, H. Ren, and J. Wang, "RIS-Aided D2D Communications Relying on Statistical CSI With Imperfect Hardware," *IEEE Communications Letters*, vol. 26, no. 2, pp. 473–477, 2022.
- [45] Q. Li, D. Xu, L. Liu, J. Du, D. Niyato, and M. Guizani, "Cooperative irls and ios-aided finite blocklength covert communications in noma networks," *IEEE Transactions on Vehicular Technology*, vol. 74, no. 2, pp. 3474–3479, 2025.
- [46] J. Zhao, G. Li, G. Chen, Q. Wu, X. Li, and J. Zhang, "Covert Communication of IRS-Assisted Wireless Networks With Stochastic Geometry Approach," *IEEE Wireless Communications Letters*, vol. 13, no. 4, pp. 974–978, 2024.
- [47] D. Wang, L. Cao, W. Shen, Z. Li, and Q. Li, "Age-of-information minimization in aerial-irls-assisted covert communication for internet of things networks," *IEEE Internet of Things Journal*, vol. 12, no. 8, pp. 9583–9595, 2025.
- [48] C. Zhang, W. Chen, Q. Chen, and C. He, "Distributed Intelligent Reflecting Surfaces-Aided Device-to-Device Communications System," *Journal of Communications and Information Networks*, vol. 6, no. 3, pp. 197–207, 2021.

- [49] C. Zhang, W. Chen, C. He, and X. Li, "Throughput Maximization for Intelligent Reflecting Surface-Aided Device-to-Device Communications System," *Journal of Communications and Information Networks*, vol. 5, no. 4, pp. 403–410, 2020.
- [50] G. Qian, Y. Zheng, W. Chen, and C. He, "Secrecy Rate Maximization for Intelligent Reflecting Surface-Assisted Device-to-Device Communications System," in *2021 IEEE 94th Vehicular Technology Conference (VTC2021-Fall)*, 2021, pp. 1–6.
- [51] M. H. Khoshafa, T. M. N. Ngatched, and M. H. Ahmed, "Reconfigurable Intelligent Surfaces-Aided Physical Layer Security Enhancement in D2D Underlay Communications," *IEEE Communications Letters*, vol. 25, no. 5, pp. 1443–1447, 2021.
- [52] K. Shahzad, X. Zhou, S. Yan, J. Hu, F. Shu, and J. Li, "Achieving Covert Wireless Communications Using a Full-Duplex Receiver," *IEEE Transactions on Wireless Communications*, vol. 17, no. 12, pp. 8517–8530, 2018.
- [53] S. Lee, R. J. Baxley, M. A. Weitnauer, and B. Walkenhorst, "Achieving Undetectable Communication," *IEEE Journal of Selected Topics in Signal Processing*, vol. 9, no. 7, pp. 1195–1205, 2015.
- [54] T. V. Sobers, B. A. Bash, S. Guha, D. Towsley, and D. Goeckel, "Covert Communication in the Presence of an Uninformed Jammer," *IEEE Transactions on Wireless Communications*, vol. 16, no. 9, pp. 6193–6206, 2017.
- [55] C. Research, "Inc. CVX: Matlab software for disciplined convex programming," version 2.0., 2011, <http://cvxr.com/cvx>.
- [56] M. Grant and S. Boyd, "Graph implementations for nonsmooth convex programs, Recent Advances in Learning and Control (a tribute to M. Vidyasagar)," *V. Blondel, S. Boyd, and H. Kimura, editors, Lecture Notes in Control and Information Sciences, Springer*, pp. 95–110, 2008, http://stanford.edu/~boyd/graph_dcp.html.
- [57] H. V. Abeywickrama, B. A. Jayawickrama, Y. He, and E. Dutkiewicz, "Potential field based inter-uav collision avoidance using virtual target relocation," in *2018 IEEE 87th Vehicular Technology Conference (VTC Spring)*, 2018, pp. 1–5.
- [58] C. Suarez-Rodriguez, Y. He, and E. Dutkiewicz, "Theoretical Analysis of REM-based Handover Algorithm for Heterogeneous Networks," *IEEE Access*, vol. 7, pp. 96 719–96 731, 2019.
- [59] S. Basnet, Y. He, E. Dutkiewicz, and B. A. Jayawickrama, "Resource Allocation in Moving and Fixed General Authorized Access Users in Spectrum Access System," *IEEE Access*, vol. 7, pp. 107 863–107 873, 2019.



Yihuai Yang received her B.E. degree in Communication Engineering from Kunming University of Science and Technology and M.S. degree in Communication and Information System from Yunnan University, China in 2001, and 2006, respectively. She is an associate professor with the School of Information Engineering, Kunming University, Yunnan, China, and also affiliated with the Academician Weiming Shen Workstation, Yunnan 650214, China. She is a member of the Yunnan Province Key Laboratory of Intelligent Logistics Equipment and

Systems, and the Yunnan Key Laboratory of Smart City and Cyberspace Security, China. Her research interests include wireless channel characteristics, wireless body networks and the Internet of Things.



Bin Yang received the Ph.D. degree in systems information science from Future University Hakodate, Hakodate, Japan, in 2015. He was a Research Fellow with the School of Electrical Engineering, Aalto University, Espoo, Finland, from November 2019 to November 2021. He is currently a professor with the School of Computer and Information Engineering, Chuzhou University, Chuzhou, China, and also with the School of Information Engineering, Kunming University, Yunnan, China. His research interests include unmanned-aerial-vehicle networks, cyber security, edge computing, and Internet of Things.



Shikai Shen received his B.S. and M.S. Degrees from Yunnan Normal University in 1984 and from Yunnan University in 2003, respectively. He is currently a Professor with the School of Information Engineering, Kunming University, Yunnan, China, and also affiliated with the Academician Weiming Shen Workstation, Yunnan 650214, China. He is a member of the Yunnan Province Key Laboratory of Intelligent Logistics Equipment and Systems, and the Yunnan Key Laboratory of Smart City and Cyberspace Security, China. He is also a Senior Member of the China Computer Federation. His research interests include wireless sensor networks, network coding, the Internet of Things, etc.



Yumei She received the B.S. degree from Minzu University of China, Peking, China, in 1985. She is currently a Professor with the Yunnan Minzu University, and Yunnan Key Laboratory of Smart City and Cyberspace Security, Kunming, China. Her research interests include natural language processing and wireless sensor networks. Prof. She is a member of the China Computer Federation. His research interests include wireless sensor networks, network coding, the Internet of Things, etc.



Xiaohong Jiang received the B.S., M.S., and Ph.D. degrees from Xidian University, China, in 1989, 1992, and 1999 respectively. He is currently a Full Professor with Future University Hakodate, Japan. Before joining Future University, he was an Associate Professor with Tohoku University, from February 2005 to March 2010. His research interests include computer communications networks, mainly wireless networks and optical networks, network security, and routers/switches design. He has published over 300 technical papers at premium international journals and conferences, which include over 70 papers published in top IEEE journals and conferences, such as IEEE/ ACM Transactions on Networking, IEEE Journal of Selected Areas on Communications, IEEE Transactions on Parallel and Distributed Systems, and IEEE INFOCOM.



Tarik Taleb received the B.E. degree (with distinction) in information engineering and the M.Sc. and Ph.D. degrees in information sciences from Tohoku University, Sendai, Japan, in 2001, 2003, and 2005, respectively. He is currently a Full Professor at Ruhr University Bochum, Germany. He was a Professor with the Center of Wireless Communications (CWC), University of Oulu, Oulu, Finland. He is the founder of ICTFICIAL Oy and the founder and Director of the MOSAIC Lab, Espoo, Finland. From October 2014 to December 2021, he was

an Associate Professor with the School of Electrical Engineering, Aalto University, Espoo, Finland. Prior to that, he worked as a Senior Researcher and a 3GPP Standards Expert with NEC Europe Ltd., Heidelberg, Germany. Before joining NEC and until March 2009, he served as an Assistant Professor with the Graduate School of Information Sciences, Tohoku University, in a lab fully funded by KDDI. From 2005 to 2006, he was a Research Fellow with the Intelligent Cosmos Research Institute, Sendai. His current research interests include AI-based network management, architectural enhancements to mobile core networks, network softwareization and slicing, mobile cloud networking, network function virtualization, software-defined networking, software-defined security, and mobile multimedia streaming.